Brain Imaging and Behavior (2019) 13:1650–1664
https://doi.org/10.1007/s11682-019-00090-y

ORIGINAL RESEARCH

Connectivity and morphology of hubs of the cerebral structural connectome are associated with brain resilience in AD- and age-related pathology

Florian U. Fischer[1,2] · Dominik Wolf[1,2] · Andreas Fellgiebel[1,2] · for the Alzheimer's Disease Neuroimaging Initiative*

Published online: 12 April 2019

Abstract

The physiological basis of resilience to age-associated and AD-typical neurodegenerative pathology is still not well understood. So far, the established resilience factor intelligence has been shown to be associated with white matter network global efficiency, a key constituent of which are highly connected hubs. However, hub properties have also been shown to be impaired in AD. Individual predisposition or vulnerability of hub properties may thus modulate the impact of pathology on cognitive outcome and form part of the physiological basis of resilience. 85 cognitively normal elderly subjects and patients with MCI with DWI, MRI and AV45-PET scans were included from ADNI. We reconstructed the global WM networks in each subject and characterized hub-properties of GM regions using graph theory by calculating regional betweenness centrality. Subsequently, we investigated whether regional GM volume (GMV) and structural WM connectivity (WMC) of more hub-like regions was more associated with resilience, quantified as cognitive performance independent of amyloid burden, tau and WM lesions. Subjects with higher resilience showed higher increased regional GMV and WMC in more hub-like compared to less hub-like GM-regions. Additionally, this association was in some instances further increased at elevated amounts of brain pathology. Higher GMV and WMC of more hub-like regions may contribute more to resilience compared to less hub-like regions, reflecting their increased importance to brain network efficiency, and may thus form part of the neurophysiological basis of resilience. Future studies should investigate the factors leading to higher GMV and WMC of hubs in non-demented elderly with higher resilience.

Keywords Hubs · Structural connectome · GM morphology · WM connectivity · Resilience · AD

Introduction

The field of neuroimaging has seen steadily rising interest in the organizational network properties of the human brain – a research topic also referred to as connectomics (Fornito et al. 2015). One major finding of related structural imaging studies has been that the brain's organizational topology exhibits prominent small-world properties, as in many natural and artificial networks (Hagmann et al. 2007). This means that white matter (WM) connections between local grey matter (GM) regions within so called clusters are on the one hand much denser than in randomly organized networks while the routes between any pair of GM regions in the network are on the other hand much shorter than one would expect from a regularly organized network (Watts and Strogatz 1998). This configuration has the benefit of minimizing metabolic cost for the upkeep of WM connections, while simultaneously

*Data used in preparation of this article were obtained from the Alzheimer's Disease Neuroimaging Initiative (ADNI) database (adni.loni.usc.edu). As such, the investigators within the ADNI contributed to the design and implementation of ADNI and/or provided data but did not participate in analysis or writing of this report. A complete listing of ADNI investigators can be found at: http://adni.loni.usc.edu/wp-content/uploads/how_to_apply/ADNI_Acknowledgement_List.pdf

Electronic supplementary material The online version of this article (https://doi.org/10.1007/s11682-019-00090-y) contains supplementary material, which is available to authorized users.

✉ Florian U. Fischer
florian.fischer@unimedizin-mainz.de

[1] Department of Psychiatry and Psychotherapy, University Medical Center Mainz, Untere Zahlbacher Str. 8, 55131 Mainz, Germany

[2] Center for Mental Health in Old Age, Landeskrankenhaus (AöR), Hartmühlenweg 2-4, 55122 Mainz, Germany

maximizing efficient information transfer capacity (Bullmore and Sporns 2012). A key feature to achieve this type of organization is a small number of highly connected hubs providing long distance connections between locally densely connected clusters of the network (Hagmann et al. 2007). As only a small number of regions in the network possess pronounced hub properties, the small world properties of the network are also theoretically robust to random insults (Albert et al. 2000). It is thus remarkable that studies have shown increased GM atrophy and WM disconnection in AD and other neurodegenerative diseases for hub regions identified from healthy anatomy (Crossley et al. 2014; Filippi et al. 2013; Fischer et al. 2015).

Given that hub GM atrophy seems to be a distinct feature of clinically manifest AD (Crossley et al. 2014), one may hypothesize that the degree of hub GM atrophy may be associated with the degree of cognitive impairment. As such, preserved GM hub volume could possibly be a resilience factor to age and AD-related brain pathology in analogy to the hippocampus (Wolf et al. 2018). There are two additional arguments to warrant the investigation of this hypothesis.

First, hub properties may be associated with cognitive performance. The organizational efficiency and robustness of the WM structural brain network is achieved by integration of locally densely connected clusters by highly connected hubs as described above (Hagmann et al. 2007). Disconnection of hubs will result in an efficiency decrease of the whole network, as has been demonstrated in AD (Lo et al. 2010). However, network efficiency is associated with intelligence (Fischer et al. 2014; Li et al. 2009), which is a known factor of resilience (Barulli and Stern 2013).

Second, there is tentative evidence that the pathomechanism by which hubs are atrophied in AD may be related to its molecular biomarker cascade. Raj et al. proposed a network diffusion model of prion-like pathogens spreading along WM fibers that predicted AD-typical GM atrophy properties from hypothetical pathogen exposure over time. As hubs are crossed by a large proportion of all possible connections across the network, it is sensible to expect early and prolonged exposure to spreading pathogens originating anywhere in the network (Raj et al. 2015). Hub atrophy may also be caused by increased disconnection vulnerability of long fiber pathways in AD (Crossley et al. 2014), to which hubs tend to be connected (Zamora-López et al. 2010). Finally, we recently demonstrated decreased structural WM connectivity of hubs in amyloid-beta positive patients with preclinical AD (Fischer et al. 2015), which may drive subsequent GM atrophy at later disease stages. Thus, if hub atrophy and disconnection are part of the pathological cascade of AD that is downstream from its early molecular biomarkers, its extent may modulate or determine the onset of the effect of these biomarkers on cognition to some degree.

Given these findings, the aim of the present study was to investigate, whether GM volume and WM structural connectivity of more hub-like regions – compared to less hub-like regions – may be more associated with resilience in people without manifest dementia that span the ranges from normal to mildly impaired cognition as well as normal to elevated levels of known markers of age- and AD-related brain pathology. To this end, resilience was statistically modelled according to its definition as the variance of cognitive outcome that could not be explained by present brain pathology (Wolf et al. 2018).

Methods

Data used in the preparation of this article were obtained from the Alzheimer's Disease Neuroimaging Initiative (ADNI) database (adni.loni.usc.edu). The ADNI was launched in 2003 as a public-private partnership, led by Principal Investigator Michael W. Weiner, MD. The primary goal of ADNI has been to test whether serial magnetic resonance imaging (MRI), positron emission tomography (PET), other biological markers, and clinical and neuropsychological assessment can be combined to measure the progression of mild cognitive impairment (MCI) and early Alzheimer's disease (AD). For up-to-date information, see www.adni-info.org.

Subjects

Subjects and their respective data points were selected from the database of the ADNI project according to the following criteria: baseline assessment during the ADNI 2 phase and classification as cognitively normal or MCI, availability of T1, FLAIR, diffusion weighted (DWI) MRI as well as florbetapir (AV45) PET imaging at baseline. MCI subjects were included so as to ensure sufficient variance of cognition and pathological markers in a continuum of elderly non-demented subjects for the assessment of possible resilience. For details regarding the cognitive assessment within the ADNI, please refer to the publicly available procedures manual: https://adni.loni.usc.edu/wp-content/uploads/2008/07/adni2-procedures-manual.pdf. In total, 85 subjects consisting of 34 females and 51 males aged 56.5 to 89.0 years were included (see Table 1 for descriptive sample characteristics).

Table 1 Sample demographics. CN: cognitively normal. MCI: mild cognitive impairment. APOE4: apolipoprotein ε4

	N	F/M	Age	Education	APOE4 ±
CN	34	18/16	73.4 ± 6.4	16.4 ± 2.6	25/9
MCI	51	16/35	72.1 ± 6.6	16.0 ± 2.7	16/35
Total group	85	34/51	72.6 ± 6.5	16.1 ± 2.7	41/44

CSF measurement

All CSF biomarkers collected at different centers were stored and analyzed at the Penn ADNI Biomarker Core Laboratory at the University of Pennsylvania, Philadelphia. CSF concentrations of total tau were measured in the baseline CSF samples using the multiplex xMAP Luminex platform (Lumnix Corp., Austin, TX). We included total tau instead of phosphorylated tau, as the latter is included in the former and also more specific to AD and thus limited in scope to AD-specific tauopathy (Blennow et al. 2001). More details on data collection and processing of the CSF samples can be found elsewhere (Shaw et al. 2009) (http://adni.loni.usc.edu/methods).

APOE genotype

Apolipoprotein (APOE) genotype was determined by genotyping the two single nucleotide polymorphisms that define the APOE ε2, ε3, and ε4 alleles (rs429358, rs7412) with DNA extracted by Cogenics from a 3-ml aliquot of EDTA blood (http://adni.loni.usc.edu/data-samples/genetic-data).

Imaging data acquisition

DWI, FLAIR and inversion-recovery spoiled gradient recalled (IR-SPGR) T1-weighted imaging data were acquired on several General Electric 3 T scanners using scanner specific protocols. Briefly, DWI data was acquired with a voxel size of $1.37^2 \times 2.70$ mm^3, 41 diffusion gradients and a b-value of 1000 s/mm^2. IR-SPGR data were acquired with a voxel size of $1.02^2 \times 1.20$mm^3.

AV45 PET imaging data were acquired on several types of scanners using different acquisition protocols. In order to increase data uniformity, the data underwent a standardized preprocessing procedure at the ADNI project. All imaging protocols and preprocessing procedures are available at the ADNI website (http://adni.loni.usc.edu/methods/).

Data processing overview

The goal of this study was to assess, whether GMV and WMC of hubs may be a resilience factor in elderly subjects without dementia. To this end, GM was first segmented using a GM-atlas. Second, the volume and the number of WM fiber connections to other GM regions was calculated, which constitute the two possible regional imaging resilience measures. Third, the hub-likeness of each GM region was calculated as the betweenness centrality of that region based on the whole-brain WM network. The following sections give details on the implementation of each step.

T1-weighted and FLAIR data processing

The T1-weighted IR-SPGR data was automatically tissue segmented and spatially normalized to MNI-space using SPM8 (http://www.fil.ion.ucl.ac.uk/spm/) and the VBM8-toolbox (http://www.neuro.uni-jena.de/vbm/). Additionally, inverse transformations from MNI to native T1 space were calculated.

Grey matter was segmented into 106 functionally and anatomically defined cortical regions as well as the subcortical basal ganglia regions as implemented in the probabilistic Harvard Oxford Atlas supplied with FSL. The volume of each region was calculated as the sum of the product of the GM-tissue segmentation probability values and the voxel size for each voxel with the highest probability of belonging to the respective region, i.e. majority voting. The probability values were modulated based on the Jacobian of affine and nonlinear components of the normalization transformation to MNI space (Ashburner and Friston 2000). GM volumes were normalized by dividing by the total intracranial volume (TIV) of the subject. Note that the different original size of atlas ROIs was modeled statistically as a random effect (see section statistical analyses).

TIV as well as WM hyperintensity volume (WMHV) were calculated at ADNI core laboratories from T1-weighted and FLAIR data using published tissue segmentation methods (DeCarli et al. 2005; Fletcher et al. 2012). WMHV was also normalized dividing by the TIV.

DWI data processing

DWI data were corrected for eddy currents and motion artefacts using the method of Rohde et al. as implemented in VistaSoft (Rohde et al. 2004). Additionally, DWI data were upsampled to 1 mm isotropic voxel size and constrained spherical deconvolution was applied. For fiber tractography, Anatomically Constrained Tractography (ACT) as implemented in MRtrix was employed (Smith et al. 2012). This approach incorporates anatomical constraints based on tissue segmentations of T1 data. To this end, VBM8 tissue segmented data in T1 native space were coregistered using SPM8 to the upsampled DWI B0 images, and used in the subsequent ACT. Based on the tissue segmentation images, the ACT framework calculates an isocontour representing the interface of GM and WM for the seeding of fibers. Subsequently, tractography seed points were placed randomly along the GM-WM interface. Starting from these points, the probabilistic "ifod2" tractography algorithm was executed until 500,000 anatomically plausible streamlines were reconstructed for each subject. Streamlines were accepted if they met the anatomical constraints of ACT (Smith et al. 2012).

Network reconstruction and characterisation

In order to reconstruct WM fibers, the Harvard Oxford Atlas GM ROIs were first warped to native T1 space using the inverse VBM8 normalization transformations and then transferred to the upsampled DWI space using the transformation estimated from the T1 to B0 coregistration. Subsequently, for each ROI pair in each subject, the number of connecting streamlines was obtained and recorded to construct the adjacency matrix, which was then binarized using a connection threshold of at least 3 connecting streamlines for each connection (Fischer et al. 2014; Li et al. 2009) as in (Crossley et al. 2014). Based on these networks, the number of white matter connections connecting to a GM region (WMC) was calculated for each GM ROI. Note that the different size of GM regions may affect the number of connections. This was modeled statistically as a random effect (see section statistical analyses). Finally, GM regions of each subject were characterized regarding their hub-like properties by calculating their betweenness centrality (BC) from the white matter networks (Crossley et al. 2014). Betweenness centrality measures the proportion of the shortest paths between each pair of GM regions across the network that passes through the GM region in question. A higher BC thus indicates that the respective GM region is more hub-like, as more connections may pass through it. For a more detailed description and discussion of graph measures see (Fornito et al. 2015). See Fig. 1 for an exemplary visualization of the reconstructed networks, Table 2 for an overview of average BC values per GM region across subjects as well as Fig. 2 for a boxplot of BC values of GM regions across subjects.

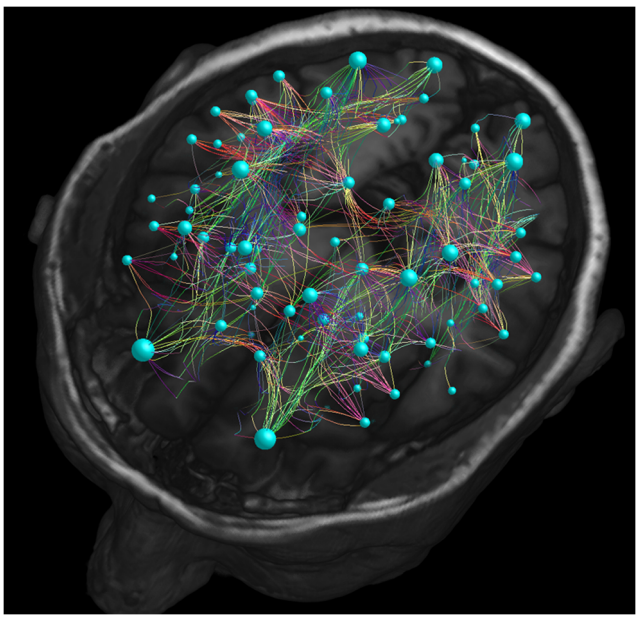

Fig. 1 Visualization of reconstructed white matter networks. Visualization of the white matter connections of a cognitively healthy amyloid negative elderly subject. Lines indicate connections and idealized orientation of reconstructed fibers within space. Line color indicates direction. Blue spheres are located at the centers of mass of grey matter atlas ROIs corresponding to the network nodes. The size of the sphere indicates the number of white matter connections (WMC) to the respective node

PET data processing

Subjects' global cortical amyloid-β load was calculated from florbetapir (AV45) PET images according to procedures established by the ADNI (http://adni.loni.usc.edu/methods/pet-analysis/). Briefly, cortical amyloid was calculated as the average of the AV45 uptake in the frontal, angular/posterior cingulate, lateral parietal and temporal cortices normalized by dividing by the mean uptake in the cerebellum.

Neuropsychological assessment and quantification of resilience

Subjects underwent an extensive neuropsychological assessment. For details regarding the cognitive assessment within the ADNI, please refer to the publicly available procedures manual: https://adni.loni.usc.edu/wp-content/uploads/2008/07/adni2-procedures-manual.pdf. Within the scope of this study, the cognitive Alzheimer's Disease Assessment Scale (ADAS-cog), which spans several cognitive domains (Rosen et al. 1984), as well as two compound scores assessing executive (EF) and memory functions (MEM) specifically were used (Crane et al. 2012; Gibbons et al. 2012).

Approach to studying resilience mechanisms

Any analysis of resilience requires at least three types of measures: a possible resilience factor, a measure of pathology and a measure of cognitive outcome (Stern 2012). However, analyses that include these three measures in regression analyses traditionally only consider an interaction between pathology and the possible resilience factor as evidence of resilience (Craik et al. 2011). Recently, we published a reconceptualization of this approach that aims to introduce a further differentiation of resilience by its relation to pathology (Wolf et al. 2018). Thus, a resilience factor may be associated with cognitive outcome with and without the presence of pathology. While this may seem trivial at first, it requires that the mechanism by which the resilience factor is associated with cognitive outcome remains intact even if pathology is present. This is termed *general resilience.* However, a resilience factor might also become more associated with cognitive outcome in the presence of more pathology, which corresponds to the traditionally common statistical modeling of resilience in the form of an interaction. This is termed *dynamic resilience*, as the role of the resilience factor depends on the amount of present pathology (for a descriptive overview of the pathology measures in the sample please see Table 3).

Table 2 Average betweenness centrality values of grey matter regions across subjects calculated from reconstructed white matter networks. Higher betweenness centrality corresponds to more hub-like properties

Grey matter region	Mean betweenness centrality	
	Left	Right
Frontal Pole	116.95	195.65
Insular Cortex	266.06	210.75
Superior Frontal Gyrus	51.94	78.59
Middle Frontal Gyrus	47.95	75.57
Inferior Frontal Gyrus, pars triangularis	13.7	16.7
Inferior Frontal Gyrus, pars opercularis	23.12	23.28
Precentral Gyrus	150.06	163.81
Temporal Pole	42.42	57.67
Superior Temporal Gyrus, anterior division	8.62	4.59
Superior Temporal Gyrus, posterior division	24.75	23.54
Middle Temporal Gyrus, anterior division	6.88	7.31
Middle Temporal Gyrus, posterior division	58.11	72.87
Middle Temporal Gyrus, temporooccipital part	54.06	69.12
Inferior Temporal Gyrus, anterior division	7.53	7.22
Inferior Temporal Gyrus, posterior division	20.28	32.94
Inferior Temporal Gyrus, temporooccipital part	19.06	43.35
Postcentral Gyrus	141.59	94.8
Superior Parietal Lobule	122.06	82.74
Supramarginal Gyrus, anterior division	36.06	19.39
Supramarginal Gyrus, posterior division	56.4	52.44
Angular Gyrus	47.35	48.73
Lateral Occipital Cortex, superior division	253.08	225.08
Lateral Occipital Cortex, inferior division	60.15	50.91
Intracalcarine Cortex	36.26	26.8
Frontal Medial Cortex	4.86	7.77
Juxtapositional Lobule Cortex (formerly Supplementary Motor Cortex)	12.35	17.23
Subcallosal Cortex	10.21	10.12
Paracingulate Gyrus	35.7	41.86
Cingulate Gyrus, anterior division	140.71	141.09
Cingulate Gyrus, posterior division	398.77	407.38
Precuneous Cortex	354.59	312.2
Cuneal Cortex	34.26	27.08
Frontal Orbital Cortex	17.31	25.56
Parahippocampal Gyrus, anterior division	3.46	2.99
Parahippocampal Gyrus, posterior division	3.05	3.52
Lingual Gyrus	13.45	26.55
Temporal Fusiform Cortex, anterior division	5.33	5.95
Temporal Fusiform Cortex, posterior division	9.67	12.06
Temporal Occipital Fusiform Cortex	6.46	10.87
Occipital Fusiform Gyrus	14.78	7.9
Frontal Operculum Cortex	4.13	6.13
Central Opercular Cortex	19.02	11.78
Parietal Operculum Cortex	48.5	38.66
Planum Polare	37	36.08
Heschl's Gyrus (includes H1 and H2)	6.02	12.02
Planum Temporale	40.4	32.74

Table 2 (continued)

Grey matter region	Mean betweenness centrality	
	Left	Right
Supracalcarine Cortex	6.05	17.44
Occipital Pole	39.78	31.55
Thalamus	437.68	364.6
Caudate	188.47	122.13
Putamen	218.49	318.64
Pallidum	58.38	82.36
Accumbens	3.14	5.4

These concepts are statistically modeled using the following equation:

$$COG \sim RES + PATH + RES*PATH$$

where COG represents the cognitive outcome measure, PATH represents a measure of pathology and RES represents a possible resilience factor. As pathology is included in this model, effects of pathology on cognitive outcome and the resilience factor are partialled out (Bortz 2013). The regression model thus estimates the association between those parts of the variance of cognitive outcome and of the resilience factor which are unexplained by pathology. This corresponds to more general definition of resilience as cognitive variance beyond what is expected based on the amount of present pathology, cognitive outcome within the context of this model will thus be referred to as resilience for improved comprehensibility in the results and discussion sections. The inclusion of the interaction term between the resilience factor and pathology additionally assesses the dependence of that association on the presence of pathology. The model is easily extended to include several measures of pathology and additional covariates.

In summary, the model supports a possible resilience factor in the following three scenarios:

(i). *General resilience factor*: Positive association of the resilience factor with resilience. No association of the interaction term RES * PATH with resilience.

This result indicates that the resilience factor is associated with resilience, irrespective of the amount of pathology.

(ii). *Dynamic resilience factor*: Significant association between the interaction term RES * PATH and resilience, such that the resilience factor is more positively associated with resilience at higher levels of the pathology measure. No main (independent) effect of the resilience factor on resilience.

This result indicates a dynamically changing association between resilience factor and resilience as a function of the amount of pathology, where the resilience factor is not associated with resilience at lower levels of pathology.

(iii). *General and dynamic resilience factor*: Significant positive main effect for the association of the resilience factor with resilience independent of pathology. Significant association between the interaction term RES * PATH and resilience, such that the resilience

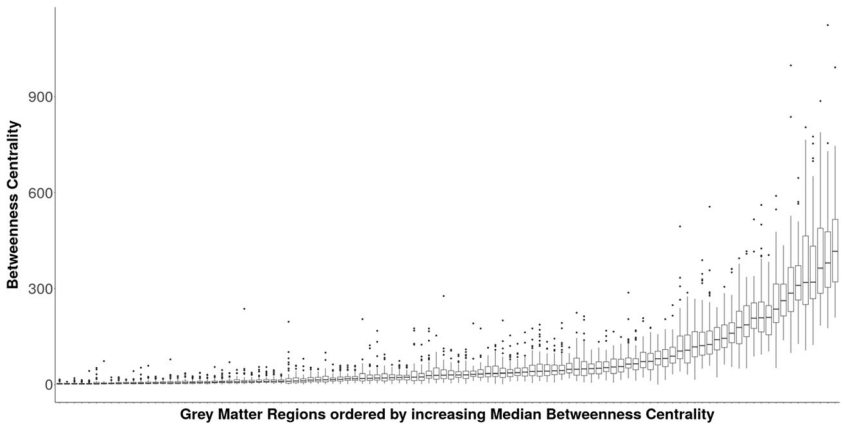

Fig. 2 Box plots of grey matter regions, ordered from left to right by increasing median betweenness centrality. Note that betweenness centrality was logarithmized for statistical analyses (see methods section)

Table 3 Descriptive statistics of cerebral pathology measures. AV45: Global florbetapir standardized uptake value ratio. TAU: liquor specimen total tau. WMHV: normalized white matter hyperintensity volume in percent

	CN	MCI	Total
AV45	1.08 ± 0.14	1.26 ± 0.24	1.19 ± 0.22
TAU	61.29 ± 23.98	98.30 ± 61.02	83.50 ± 52.68
WMHV	0.38 ± 0.28	0.58 ± 0.57	0.53 ± 0.49

factor is positively related to resilience where the strength of this association is higher at high levels of pathology. This result indicates that a significant part of the association of the resilience factor with resilience is independent of the amount of pathology. However, the strength of this association dynamically increases at higher levels of pathology.

The concepts of general and dynamic resilience overlap but are not equivalent to the concept of brain reserve and cognitive reserve put forward by (Barulli and Stern 2013): whereas the definitions of brain reserve and cognitive reserve refer to the quality of the underlying mechanism of resilience, the concept of general and dynamic resilience is based entirely on the empirical manifestation of resilience as associations with the resilience factor (Wolf et al. 2018). Brain reserve could thus manifest as general resilience or dynamic resilience (e.g. dynamic in the case of a threshold based association), as might cognitive reserve (which may have a positive effect on cognition even in the absence of pathology).

Statistical analyses

Model adaption

The present study investigates whether GMV and WMC of more hub-like GM regions are more associated with resilience. As GMV and WMC are based on differently sized ROIs and span several data points per subject, random effects per ROI and per subject need to be modeled. Additionally, spatial autocorrelation of model residuals needs to be controlled. To this end, we employed linear mixed effects models (LMM) for data analysis, which required an adaption of the resilience model described in the previous section. The position of the resilience factors, GMV and WMC, and cognitive outcome need to be interchanged in order to put GMV and WMC data as dependent variables for the controling of random effects. In the case of general resilience, this would have no effect on the estimation of the association between resilience factor and cognitive outcome in ordinary least squares multiple regression analysis, since the residual variance of the dependent variable and predictor after removing the effects of all other predictors are used for estimation of partial regression coefficients (PRC) (Bortz 2013). The numerical difference of PRCs after the interchange of a predictor and the dependent variable would refer merely to the different scaling of the coefficient by the variance of the variables (Bortz 2013). For this reason, cognitive outcome can in principle still be refered to as resilience. However, within the context of dynamic resilience, the interchange results in an interaction term that is the product of cognitive outcome and pathology as opposed to the product of resilience factor and pathology as in the original modeling approach and thus acquires a slightly different meaning. This will be taken into account within the limitation section of the discussion.

Model details

In order to investigate, whether regional GMV and WMC of more hub-like GM regions were more associated with resilience than less hub-like GM regions, the following linear mixed effects models were estimated:

Regional Grey Matter Volume of Hubs - General Resilience

(a)

$$\mathrm{GMV}\sim \mathrm{COG} + \mathrm{BC} + \mathit{COG}{*}\mathit{BC} + \mathrm{AV45} + \mathrm{TAU} + \mathrm{WMHV} + (1|\mathrm{ROI}) + (1|\mathrm{SUB})$$

Regional Grey Matter Volume of Hubs - Dynamic Resilience

(b)

$$\mathrm{GMV}\sim \mathrm{COG} + \mathrm{BC} + \mathrm{COG}{*}\mathrm{BC} + \mathrm{COG}{*}\mathrm{AV45} + \mathrm{BC}{*}\mathrm{AV45} + \mathit{COG}{*}\mathit{BC}{*}\mathit{AV}45 + \mathrm{AV45} + \mathrm{TAU} + \mathrm{WMHV} + (1|\mathrm{ROI}) + (1|\mathrm{SUB})$$

(c)

$$\mathrm{GMV}\sim \mathrm{COG} + \mathrm{BC} + \mathrm{COG}{*}\mathrm{BC} + \mathrm{COG}{*}\mathrm{TAU} + \mathrm{BC}{*}\mathrm{TAU} + \mathit{COG}{*}\mathit{BC}{*}\mathit{TAU} + \mathrm{AV45} + \mathrm{TAU} + \mathrm{WMHV} + (1|\mathrm{ROI}) + (1|\mathrm{SUB})$$

(d)

$$\mathrm{GMV}\sim \mathrm{COG} + \mathrm{BC} + \mathrm{COG}{*}\mathrm{BC} + \mathrm{COG}{*}\mathrm{WMHV} + \mathrm{BC}{*}\mathrm{WMHV} + \mathit{COG}{*}\mathit{BC}{*}\mathit{WMVH} + \mathrm{AV45} + \mathrm{TAU} + \mathrm{WMHV} + (1|\mathrm{ROI}) + (1|\mathrm{SUB})$$

Regional White Matter Connectivity of Hubs - General Resilience

(e)

$$\mathrm{WMC}\sim\mathrm{COG} + \mathrm{BC} + \mathit{COG}*\mathit{BC} + \mathrm{AV45} + \mathrm{TAU} + \mathrm{WMHV} + (1|\mathrm{ROI}) + (1|\mathrm{SUB})$$

Regional White Matter Connectivity - Dynamic Resilience

(f)

$$\mathrm{WMC}\sim\mathrm{COG} + \mathrm{BC} + \mathrm{COG}*\mathrm{BC} + \mathrm{COG}*\mathrm{AV45} + \mathrm{BC}*\mathrm{AV45} + \mathit{COG}*\mathit{BC}*\mathit{AV45} + \mathrm{AV45} + \mathrm{TAU} + \mathrm{WMHV} + (1|\mathrm{ROI}) + (1|\mathrm{SUB})$$

(g)

$$\mathrm{WMC}\sim\mathrm{COG} + \mathrm{BC} + \mathrm{COG}*\mathrm{BC} + \mathrm{COG}*\mathrm{TAU} + \mathrm{BC}*\mathrm{TAU} + \mathit{COG}*\mathit{BC}*\mathit{TAU} + \mathrm{AV45} + \mathrm{TAU} + \mathrm{WMHV} + (1|\mathrm{ROI}) + (1|\mathrm{SUB})$$

(h)

$$\mathrm{WMC}\sim\mathrm{COG} + \mathrm{BC} + \mathrm{COG}*\mathrm{BC} + \mathrm{COG}*\mathrm{WMHV} + \mathrm{BC}*\mathrm{WMHV} + \mathit{COG}*\mathit{BC}*\mathit{WMVH} + \mathrm{AV45} + \mathrm{TAU} + \mathrm{WMHV} + (1|\mathrm{ROI}) + (1|\mathrm{SUB})$$

where GMV refers to grey matter volume, WMC to white matter connectivity, COG to cognitive outcome (ADAS-cog, EF and MEM), BC to betweenness centrality (i.e. hub-likeness of the respective ROI), AV45 to global amyloid burden, TAU to total corticospinal fluid tau and WMHV to white matter hyperintensity volume. The terms (1|ROI) and (1|SUB) refer to a random intercept estimated for each ROI and for each subject (crossed random effects). Terms of interest (in italics) were in the case of general resilience the first order interaction term COG * BC - whether GMV or WMC of more hub-like GM regions was more associated with cognitive performance unexplained by pathology - and in the case of dynamic resilience the second order interaction term COG * BC * pathology (whether GMV or WMC of more hub-like regions was more associated with cognitive performance unexplained by pathology at elevated amounts of pathology).

For significance testing, these models as well as a corresponding reduced model each with the respective term of interest removed were estimated using maximum likelihood. Each model was then compared to its reduced counterpart using AIC. If the difference of the AIC of reduced model minus the full model was at least 10, significance testing was carried out using likelihood ratio test (LRT). For the reporting of regression coefficients of models with significant terms of interest, the respective models were reestimated using restricted maximum likelihood. These models were also reestimated using robust linear mixed effects models (RLMM) for coefficient comparison. Additionally, Moran's I-test was used to test for residual autocorrelation.

For all full models, age was entered as a covariate. Additionally, gender, years of education, APOE-4 positivity and clinical status (CN or MCI) were considered as potential covariates. All models were thus estimated first without these potential covariates well as with all possible combinations of them. Finally, AIC was used to select the respective appropriate combination of covariates for each model. Reduced models included the same combination of covariates as the full models.

All statistical analyses were conducted using R 3.4.0 as well as the packages" lme4 "(Bates et al. 2014)," robustlmm "(Koller 2016)," robustbase "(Todorov and Filzmoser 2009) and" ape "(Paradis et al. 2004). Data points with implausible measurements derived from imaging data, i.e. regional GMV, WMC and BC, were dropped. All variables that were part of an interaction term in any model were centered to reduce collinearity (Aiken et al. 1991). BC and WMHV were log-transformed to achieve approximate normal distribution. The significance threshold was set to $\alpha = 0.05$ for all analyses. Additionally, the Holm-Bonferroni method was applied to control the family wise error rate (Holm 1979).

Results

For an overview of estimated model parameters, please refer to Table 4. For a visualization of the estimated terms of interest as well as scatter plots of the data, please see Figs. 3 and 4.

For models of general resilience, AIC indicated a better fit for the full models including the interaction term of resilience and BC compared to reduced models, for both GMV and WMC and across cognitive outcome measures (ΔAIC between 33.86 and 82.68), with the exception of MEM for WMC (ΔAIC -.85). The corresponding p values calculated by means of LRT for all general resilience models with ΔAIC greater than 10 were all smaller than .00001. The estimated significant interactions were such that resilience, i.e. cognitive outcome controlled for pathology measures, was more associated with GMV and WMC of GM regions with higher BC, i.e. more hub-like properties. The significant estimated standardized betas ranged between .0110 and .0234. Robust reestimation of these models yielded coefficients of similar magnitude and directionality between .0084 and .0221 for the interaction term.

Table 4 Model estimates and results. ΔAIC: Difference of Akaike's Information Criterion of the reduced model without the term of interest and the full model. Beta: standardized regression coefficient. Robust beta: robust standardized regression coefficient. LRT: likelihood ratio test. GMV: normalized regional grey matter volume. WMC: number of regional white matter connections. ADAS-cog: Alzheimer's Disease Assessment Scale. EF: Executive function compound score. MEM: memory function compound score. BC: regional betweenness centrality derived from individual white matter networks. AV45: amyloid burden quantified by florbetapir PET. TAU: liquor specimen total tau. WMHV: normalized white matter hyperintensity volume

Dependent variable	Term of interest	ΔAIC	Beta	Robust beta	LRT Chi^2	*P*-value
GMV	ADAS * BC	65.28	0.0149	0.0104	67.28	<0.00001*
	ADAS * AV45 * BC	33.39	0.0129	0.0112	35.39	<0.00001*
	ADAS * TAU * BC	22.25	0.0124	0.0103	24.25	<0.00001*
	ADAS * WMHV * BC	−1.68				
	EF * BC	33.86	0.0110	0.0084	35.86	<0.00001*
	EF * AV45 * BC	5.52				
	EF * TAU * BC	−0.68				
	EF * WMHV * BC	0.18				
	MEM * BC	70.59	0.0154	0.0103	72.59	<0.00001*
	MEM * AV45 * BC	17.81	0.0114	0.0099	19.81	<0.00001*
	MEM * TAU * BC	−1.13				
	MEM * WMHV * BC	−1.35				
WMC	ADAS * BC	44.06	0.0171	0.0173	46.06	<0.00001*
	ADAS * AV45 * BC	6.46				
	ADAS * TAU * BC	−1.96				
	ADAS * WMHV * BC	−0.57				
	EF * BC	82.68	0.0234	0.0221	84.68	<0.00001*
	EF * AV45 * BC	3.39				
	EF * TAU * BC	27.97	−0.0139	−0.0169	29.97	<0.00001*
	EF * WMHV * BC	99.05	0.0246	0.0256	101.05	<0.00001*
	MEM * BC	−0.85				
	MEM * AV45 * BC	2.58				
	MEM * TAU * BC	0.44				
	MEM * WMHV * BC	23.69	0.0133	0.0156	25.69	<0.00001*

*Statistically significant

For models of dynamic resilience, the results were more varied. For GMV, AIC indicated a better fit for the full models including the second order interaction term of resilience with BC and AV45 for the cognitive outcome measures ADAS-cog and MEM (ΔAIC 33.39 and 17.81, respectively), as well as the interaction term of resilience with BC and tau for the cognitive outcome measure ADAS-cog (ΔAIC 22.25). The corresponding p values calculated by means of LRT were all below .00001. These interactions were such that dynamic resilience for amyloid and tau, i.e. cognitive performance unexplained by pathology at increased amounts of global amyloid burden or CSF total tau, was more associated with GMV of GM regions with higher BC values. The significant estimated standardized betas ranged between .0114 and .0129. Robust reestimation of these models yielded coefficients of similar magnitude and directionality for the interaction term between .0099 and .0112.

For WMC, AIC indicated a better fit for the full models including the second order interaction term of resilience with BC and WMHV for the cognitive outcome measures EF and MEM (ΔAIC 99.05 and 23.69, respectively), as well as the interaction term of resilience with BC and tau for the cognitive outcome measure EF (ΔAIC 27.97). The corresponding *p*-values calculated by means of LRT were all below .00001. These interactions were different for WMHV and tau: dynamic resilience at increased amounts of WMHV was more associated with WMC of GM regions with higher BC for the cognitive outcome measures EF and MEM. In contrast, dynamic resilience at increased amounts of CSF total tau was less associated with WMC of GM regions with higher BC values for the cognitive outcome measure EF. The significant estimated standardized betas for WMHV were .0246 for EF and .0133 for MEM, as well as for tau −.0139 for EF. Robust reestimation of these models yielded coefficients of

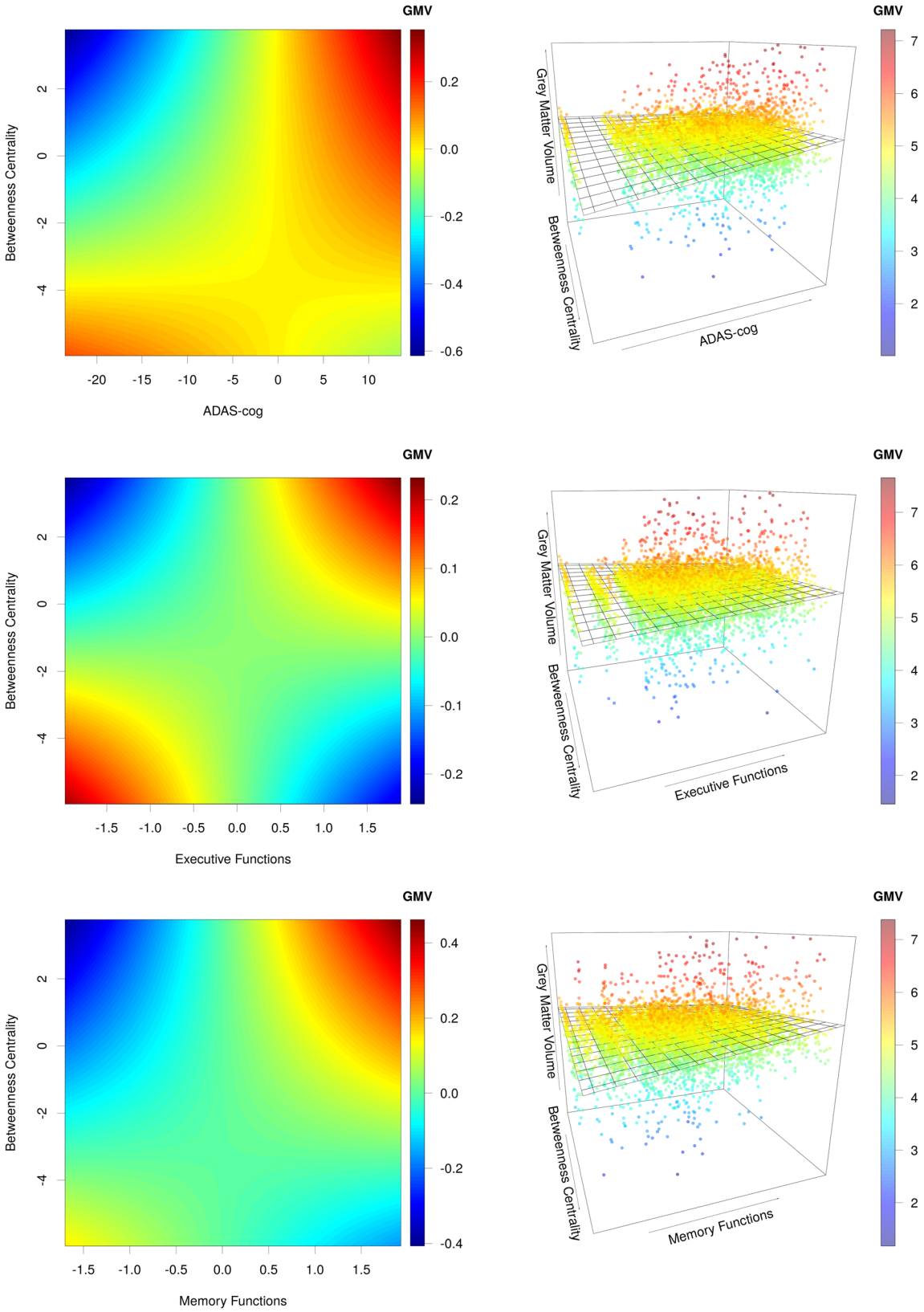

similar magnitude and directionality for the interaction term (for WMHV .0256 for EF and .0156 for MEM as well as for tau −.0169 for EF).

All statistically significant main results survived the family wise error correction according to Bonferroni. Moran‘s I did not show significantly auto correlated

◀ **Fig. 3** Higher Association of Grey Matter Volume of more Hub-like Grey Matter Regions with General Resilience. Left column: visualization of the shape of the estimated association of resilience, i.e. cognitive outcome controlled for pathology, and regional grey matter volume modulated by betweenness centrality (BC), i.e. hub-likeness. GMV: sum of estimated regression coefficients of cognitive outcome and the interaction of cognitive outcome and BC both multiplied with respective values from a parameter grid representing the data-range. Note that the main effect of BC is not considered. Cognitive outcome and BC were demeaned, ADAS-cog was inverted. Right column, GMV: scatter plot of the residual variance of regional grey matter volumes – after partialling out the estimated random effects, covariates and the main effect of BC as well as removing 0.1% of most extreme values – with the overlayed regression surface from the left column, representing the BC-modulated association with resilience. The upper edge of the left column plots corresponds to the frontal edge of the regression surface in the right column plots

residuals for the general resilience models (*p*-values between .36655 and .74474). Apart from age, additional covariates selected for the models via AIC were years of education for the dynamic resilience model including GMV, ADAS-cog and amyloid load, years of education and clinical status (CN/MCI) for the general and all dynamic resilience models including GMV and EF as well as years of education for the dynamic resilience model including GMV, MEM and tau.

Discussion

The main results of this study indicate that better cognitive performance than expected based on brain pathology generally was more associated with GMV and WMC of more hub-like GM regions compared to less hub-like GM regions. Or equivalently, general resilience was more associated with GMV and WMC of more hub-like GM regions. Additionally, in some instances the higher association of cognitive performance unexplained by brain pathology with GMV and WMC at increased amounts of brain pathology compared to less amounts was further increased for more hub-like GM regions compared to less hub-like GM regions. Or equivalently, dynamic resilience was more associated with GMV and WMC of more hub-like GM regions – specifically, for GMV at higher amyloid burden as well as at higher amounts of CSF tau, and for WMC at higher WMHV. However, in one instance dynamic resilience at higher levels of CSF tau was less associated with WMC in more hub-like GM regions.

To our best knowledge, properties of hubs characterized using graph theory have not been investigated for their association with resilience before. However, higher brain volume as well as regional GMV have been demonstrated to be associated with resilience (Arenaza-Urquijo et al. 2013; Bartrés-Faz et al. 2009; Barulli and Stern 2013). Microstructural WM properties as well as WM network efficiency have been shown to be associated with known proxy measures of resilience such as intelligence and education (Deary et al. 2010; Fischer et al. 2014; Li et al. 2009; Teipel et al. 2009; Wook Yoo et al. 2015). The association of WM network efficiency and intelligence shown previously lends a starting point for a possible explanation of the higher association of more hub-like GM regions‘properties with resilience. FMRI studies show that solving increasingly demanding cognitive tasks, as are found in intelligence assessment, is generally accompanied by synchronized activation of more GM regions, which in turn depends upon WM properties (Deary et al. 2010). It is thus a plausible assumption that more efficient WM organization will enable more efficient and/or effective information transfer and synchronized distributed information processing, leading to better performance in subjects. Furthermore, the WM network efficiency is dependent upon the prominent small world characteristics of the network, a key feature of which are short paths between any pair of nodes, i.e. GM regions, in the network. Short paths, in turn, are provided by highly connected hub regions, which connect clusters of interconnected GM regions via long distance fiber paths (Bullmore and Sporns 2012; M. P. van den Heuvel and Sporns 2013). As intelligence is a known factor for resilience (Barulli and Stern 2013), it follows that hub properties are likely to be more associated with resilience as well. The results of the present study are in support of this hypothesis. More specifically, as high WM structural connectivity of hub regions is a key factor of WM network efficiency, the finding of a higher association with resilience is in line with the hypothesis stated above. Concerning hub GMV, one may expect that not only connectivity of hubs has an effect on the efficacy of synchronized information processing but also the integrity of the hub‘s GM, of which volume is a common surrogate marker. The implicit hypothesis is that as information passes from one GM region to another via the hub as predicted by the hub‘s high BC measure, some form of relaying, reencoding and/or processing may take place that depends on the integrity of the hub‘s GMV. Since the WM network architecture predicts a sizeable proportion of possible connections to pass through hub regions (quantified by BC), which is supported by findings of higher functional activity and connectivity in hubs in healthy subjects (Liang et al. 2013; Tomasi et al. 2013), it follows that GMV of more hub-like regions may be more associated with resilience. The findings of the present study lend support to this hypothesis.

Furthermore, in addition to the higher association of general resilience with regional GMV and WMC in more hub-like regions, our results indicate that in some instances dynamic resilience is also more associated with GMV and WMC of more hub-like regions. For GMV, this was the case at increased levels of cerebral amyloid burden when considering ADAS-cog and MEM, as well as at increased levels of CSF tau when considering ADAS-cog. Amyloidosis has been

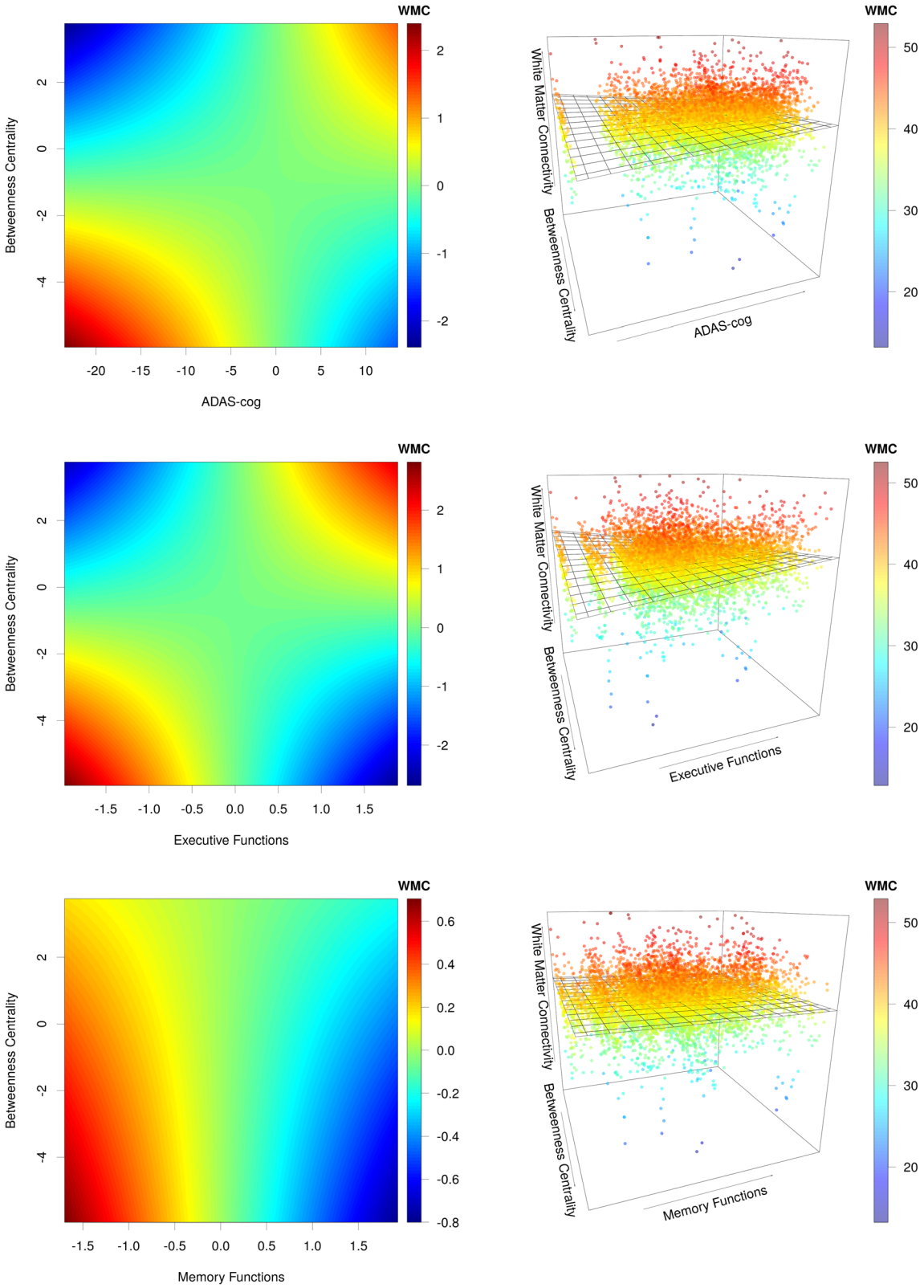

shown to be concomitant with increased neuronal activity, which may refer to compensatory mechanisms (Stargardt et al. 2015). Recruitment of additional neural networks in aging at higher load has been shown by several fMRI studies (Reuter-Lorenz and Park 2014). It is probable that the efficacy and efficiency of these more widely distributed networks depends upon hub integrity, for which GMV may be a surrogate. Furthermore, there is some evidence that lesions associated

◀ **Fig. 4** Higher Association of White Matter Connectivity of more Hub-like Grey Matter Regions with General Resilience. Left column: visualization of the shape of the estimated association of resilience, i.e. cognitive outcome controlled for pathology, and regional white matter connectivity modulated by betweenness centrality (BC), i.e. hub-likeness. WMC: sum of estimated regression coefficients of cognitive outcome and the interaction of cognitive outcome and BC both multiplied with respective values from a parameter grid representing the data-range. Note that the main effect of BC is not considered. Cognitive outcome and BC were demeaned, ADAS-cog was inverted. Right column, WMC: scatter plot of the residual variance of regional white matter connectivity – after partialling out the estimated random effects, covariates and the main effect of BC as well as removing 0.1% of most extreme values – with the overlayed regression surface from the left column, representing the BC-modulated association with resilience. The upper edge of the left column plots corresponds to the frontal edge of the regression surface in the right column plots

with neurosurgery on the brain lead to higher load of activity in hub regions (Carbo et al. 2017), which possibly refers to compensatory activity as well. As CSF tau is an established marker of neurodegeneration, compensatory activity due to neurodegeneration may be dependent on GM hub integrity as well, as in the case of amyloidosis. Recruitment of neural resources via expanded or altered functional networks and corresponding increased hub activity may be an explanation for the increased association of GMV of more hub-like regions with dynamic resilience.

In contrast to GMV, WMC of more hub-like GM regions was less associated with dynamic resilience at increased CSF tau when considering EF. This is the only model, where properties of more hub-like GM regions were less associated with resilience and thus seemingly counterintuitive. However, a possible explanation is provided by the recent finding that WMC of hubs is impaired already at the preclinical stage of AD, i.e. in asymptomatic subjects with cerebral amyloidosis (Fischer et al. 2015). At elevated amounts of CSF tau, which chronologically follows cerebral amyloid deposition in the biomarker cascade of AD (Jack et al. 2013), the process of WMC impairment of specifically more hub-like GM regions may be too advanced for it to benefit compensatory activity involving hub-like GM regions. In contrast, GMV of more hub-like GM regions has only been shown to be impaired at the dementia stage of AD (Crossley et al. 2014). Finally, the fact that WMC of more hub-like GM regions is more associated with dynamic resilience at increased WMHV when considering both EF and MEM is consistent with this view, as white matter lesions are an age-associated rather than AD-specific pathology. As increased WMHV impairs the information transfer between distributed functional networks of the brain, white matter lesions are associated with an overall slowing of processing speed (D. M. J. van den Heuvel et al. 2006). The effectiveness of putative compensatory rerouting via alternative WM pathways may be increased by higher WMC of more hub-like GM regions, which are essential to overall network integration and efficiency (Hagmann et al. 2007) – thus being more associated with dynamic resilience than less hub-like GM regions.

Finally, regarding the results with respect to the different cognitive outcome measures used for the modelling of resilience in this study, there is a striking difference between models of general and of dynamic resilience. Higher association of properties of more hub-like GM regions with general resilience is consistent across cognitive outcome measures with the exception of WMC and MEM – one might thus generalize that higher WMC and GMV of more hub-like GM regions is more beneficial for general resilience across several cognitive domains. Regarding dynamic resilience, however, the higher association of properties of more hub-like GM regions seems to be generally more limited to specific combinations of the properties of the more hub-like GM regions and the cognitive and pathology measures considered for dynamic resilience.

This study has several limitations. First, the sample size of 85 subjects is rather small in order to draw conclusions about the general population. However, this should not be a problem regarding the data analysis methodology, as there are around 106 data points per subject available for model estimation. Second, the study sample is divergent in a number of aspects from the general population regarding ethnicity, education, familial history of AD and memory impairment within the MCI group, thus limiting generalization further. Third, the cross sectionality of the analysis does not allow the inference of causality. Fourth, as discussed in the model adaption section, the flipping of the dependent and independent variable part of an interaction term may lead to slightly different estimates due to the differently calculated interaction term. However, the supplementary material to this article includes a calculation with regard to this matter.

Conclusion

Preserved GMV and WMC of more hub-like GM regions are more associated with resilience, i.e. better cognitive function in individuals than expected based on cerebral pathology. Additionally, elevated amounts of brain pathology may in some instances increase the contribution of GMV and WMC of more hub-like GM regions to resilience. Future studies should aim to investigate the factors that determine inter-individual variance of hub GMV and WMC in normal aging and disease with the ultimate goal of designing possible intervention strategies to strengthen the cerebral structural connectome‘s resilience capacity.

Acknowledgements Data collection and sharing for this project was funded by the Alzheimer’s Disease Neuroimaging Initiative (ADNI) (National Institutes of Health Grant U01 AG024904) and DOD ADNI (Department of Defense award number W81XWH-12-2-0012). ADNI is

funded by the National Institute on Aging, the National Institute of Biomedical Imaging and Bioengineering, and through generous contributions from the following: AbbVie, Alzheimer's Association; Alzheimer's Drug Discovery Foundation; Araclon Biotech; BioClinica, Inc.; Biogen; Bristol-Myers Squibb Company; CereSpir, Inc.; Cogstate; Eisai Inc.; Elan Pharmaceuticals, Inc.; Eli Lilly and Company; EuroImmun; F. Hoffmann-La Roche Ltd. and its affiliated company Genentech, Inc.; Fujirebio; GE Healthcare; IXICO Ltd.; Janssen Alzheimer Immunotherapy Research & Development, LLC.; Johnson & Johnson Pharmaceutical Research & Development LLC.; Lumosity; Lundbeck; Merck & Co., Inc.; Meso Scale Diagnostics, LLC.; NeuroRx Research; Neurotrack Technologies; Novartis Pharmaceuticals Corporation; Pfizer Inc.; Piramal Imaging; Servier; Takeda Pharmaceutical Company; and Transition Therapeutics. The Canadian Institutes of Health Research is providing funds to support ADNI clinical sites in Canada. Private sector contributions are facilitated by the Foundation for the National Institutes of Health (www.fnih.org). The grantee organization is the Northern California Institute for Research and Education, and the study is coordinated by the Alzheimer's Therapeutic Research Institute at the University of Southern California. ADNI data are disseminated by the Laboratory for Neuro Imaging at the University of Southern California.

Compliance with ethical standards

Conflict of interest Author Florian U. Fischer, Author Dominik Wolf and Author Andreas Fellgiebel declare that they have no conflict of interest.

Informed consent All procedures followed were in accordance with the ethical standards of the responsible committee on human experimentation (institutional and national) and with the Helsinki Declaration of 1975, and the applicable revisions at the time of the investigation. Informed consent was obtained from all patients for being included in the study.

Non-animal research No animal studies were carried out by the authors for this article.

References

Aiken, L. S., West, S. G., & Reno, R. R. (1991). *Multiple regression: Testing and interpreting interactions*. SAGE.

Albert, R., Jeong, H., & Barabási, A.-L. (2000). Error and attack tolerance of complex networks. *Nature, 406*(6794), 378–382. https://doi.org/10.1038/35019019.

Arenaza-Urquijo, E. M., Landeau, B., La Joie, R., Mevel, K., Mézenge, F., Perrotin, A., et al. (2013). Relationships between years of education and gray matter volume, metabolism and functional connectivity in healthy elders. *NeuroImage, 83*, 450–457. https://doi.org/10.1016/j.neuroimage.2013.06.053.

Ashburner, J., & Friston, K. J. (2000). Voxel-based morphometry—The methods. *NeuroImage, 11*(6), 805–821. https://doi.org/10.1006/nimg.2000.0582.

Bartrés-Faz, D., Solé-Padullés, C., Junqué, C., Rami, L., Bosch, B., Bargalló, N., Falcón, C., Sánchez-Valle, R., & Molinuevo, J. L. (2009). Interactions of cognitive reserve with regional brain anatomy and brain function during a working memory task in healthy elders. *Biological Psychology, 80*(2), 256–259. https://doi.org/10.1016/j.biopsycho.2008.10.005.

Barulli, D., & Stern, Y. (2013). Efficiency, capacity, compensation, maintenance, plasticity: Emerging concepts in cognitive reserve. *Trends in Cognitive Sciences, 17*(10), 502–509. https://doi.org/10.1016/j.tics.2013.08.012.

Bates, D., Mächler, M., Bolker, B., & Walker, S. (2014). Fitting Linear Mixed-Effects Models using lme4. Retrieved from https://arxiv.org/abs/1406.5823

Blennow, K., Vanmechelen, E., & Hampel, H. (2001). CSF total tau, Aβ42 and phosphorylated tau protein as biomarkers for Alzheimer's disease. *Molecular Neurobiology, 24*(1), 87–098. https://doi.org/10.1385/MN:24:1-3:087.

Bortz, J. (2013). *Statistik: Für Sozialwissenschaftler*. Springer-Verlag.

Bullmore, E., & Sporns, O. (2012). The economy of brain network organization. *Nature Reviews Neuroscience, 13*(5), 336–349. https://doi.org/10.1038/nrn3214.

Carbo, E. W. S., Hillebrand, A., van Dellen, E., Tewarie, P., de Witt Hamer, P. C., Baayen, J. C., Klein, M., Geurts, J. J. G., Reijneveld, J. C., Stam, C. J., & Douw, L. (2017). Dynamic hub load predicts cognitive decline after resective neurosurgery. *Scientific Reports, 7*, 42117. https://doi.org/10.1038/srep42117.

Craik, F. I. M., Salthouse, T. A., & Salthouse, T. A. (2011, March 15). Intelligence, education, and the brain reserve hypothesis: Helen Christensen, Kaarin J. Anstey, Liana S. Leach, and Andrew J. Mackinnon. https://doi.org/10.4324/9780203837665-9.

Crane, P. K., Carle, A., Gibbons, L. E., Insel, P., Mackin, R. S., Gross, A., et al. (2012). Development and assessment of a composite score for memory in the Alzheimer's Disease Neuroimaging Initiative (ADNI). *Brain Imaging and Behavior, 6*(4), 502–516. https://doi.org/10.1007/s11682-012-9186-z.

Crossley, N. A., Mechelli, A., Scott, J., Carletti, F., Fox, P. T., Mcguire, P., & Bullmore, E. T. (2014). The hubs of the human connectome are generally implicated in the anatomy of brain disorders. *Brain, 137*(8), 2382–2395. https://doi.org/10.1093/brain/awu132.

Deary, I. J., Penke, L., & Johnson, W. (2010). The neuroscience of human intelligence differences. *Nature Reviews Neuroscience, 11*(3), 201–211. https://doi.org/10.1038/nrn2793.

DeCarli, C., Fletcher, E., Ramey, V., Harvey, D., & Jagust, W. J. (2005). Anatomical mapping of white matter hyperintensities (WMH): Exploring the relationships between periventricular WMH, deep WMH, and total WMH burden. *Stroke, 36*(1), 50–55. https://doi.org/10.1161/01.STR.0000150668.58689.f2.

Filippi, M., Heuvel, M. P. van den, Fornito, A., He, Y., Pol, H. E. H., Agosta, F., … Rocca, M. A. (2013). Assessment of system dysfunction in the brain through MRI-based connectomics. *The Lancet Neurology, 12*(12), 1189–1199. https://doi.org/10.1016/S1474-4422(13)70144-3.

Fischer, F. U., Wolf, D., Scheurich, A., & Fellgiebel, A. (2014). Association of Structural Global Brain Network Properties with intelligence in Normal aging. *PLoS One, 9*(1), e86258. https://doi.org/10.1371/journal.pone.0086258.

Fischer, F. U., Wolf, D., Scheurich, A., & Fellgiebel, A. (2015). Altered whole-brain white matter networks in preclinical Alzheimer's disease. *NeuroImage: Clinical, 8*, 660–666. https://doi.org/10.1016/j.nicl.2015.06.007.

Fletcher, E., Singh, B., Harvey, D., Carmichael, O., & DeCarli, C. (2012). Adaptive image segmentation for robust measurement of longitudinal brain tissue change. In *2012 Annual International Conference of the IEEE Engineering in Medicine and Biology Society* (pp. 5319–5322). https://doi.org/10.1109/EMBC.2012.6347195.

Fornito, A., Zalesky, A., & Breakspear, M. (2015). The connectomics of brain disorders. *Nature Reviews Neuroscience, 16*(3), 159–172. https://doi.org/10.1038/nrn3901.

Gibbons, L. E., Carle, A. C., Mackin, R. S., Harvey, D., Mukherjee, S., Insel, P., … Initiative, for the A. D. N. (2012). A composite score for executive functioning, validated in Alzheimer's Disease Neuroimaging Initiative (ADNI) participants with baseline mild cognitive impairment. *Brain Imaging and Behavior, 6*(4), 517–527. https://doi.org/10.1007/s11682-012-9176-1.

Hagmann, P., Kurant, M., Gigandet, X., Thiran, P., Wedeen, V. J., Meuli, R., & Thiran, J.-P. (2007). Mapping human whole-brain structural networks with diffusion MRI. *PLoS One, 2*(7), e597. https://doi.org/10.1371/journal.pone.0000597.

Holm, S. (1979). A simple sequentially Rejective multiple test procedure. *Scandinavian Journal of Statistics, 6*(2), 65–70.

Jack, C. R., Knopman, D. S., Jagust, W. J., Petersen, R. C., Weiner, M. W., Aisen, P. S., … Trojanowski, J. Q. (2013). Tracking pathophysiological processes in Alzheimer's disease: An updated hypothetical model of dynamic biomarkers. *The Lancet Neurology, 12*(2), 207–216. https://doi.org/10.1016/S1474-4422(12)70291-0.

Koller, M. (2016). Robustlmm: An R package for robust estimation of linear mixed-effects models. *Journal of Statistical Software*. https://doi.org/10.18637/jss.v075.i06.

Li, Y., Liu, Y., Li, J., Qin, W., Li, K., Yu, C., & Jiang, T. (2009). Brain anatomical network and intelligence. *PLoS Computational Biology, 5*(5), e1000395. https://doi.org/10.1371/journal.pcbi.1000395.

Liang, X., Zou, Q., He, Y., & Yang, Y. (2013). Coupling of functional connectivity and regional cerebral blood flow reveals a physiological basis for network hubs of the human brain. *Proceedings of the National Academy of Sciences, 110*(5), 1929–1934. https://doi.org/10.1073/pnas.1214900110.

Lo, C.-Y., Wang, P.-N., Chou, K.-H., Wang, J., He, Y., & Lin, C.-P. (2010). Diffusion tensor Tractography reveals abnormal topological Organization in Structural Cortical Networks in Alzheimer's disease. *Journal of Neuroscience, 30*(50), 16876–16885. https://doi.org/10.1523/JNEUROSCI.4136-10.2010.

Paradis, E., Claude, J., & Strimmer, K. (2004). APE: Analyses of Phylogenetics and evolution in R language. *Bioinformatics (Oxford, England), 20*(2), 289–290.

Raj, A., LoCastro, E., Kuceyeski, A., Tosun, D., Relkin, N., & Weiner, M. (2015). Network diffusion model of progression predicts longitudinal patterns of atrophy and metabolism in Alzheimer's disease. *Cell Reports, 10*(3), 359–369. https://doi.org/10.1016/j.celrep.2014.12.034.

Reuter-Lorenz, P. A., & Park, D. C. (2014). How does it STAC up? Revisiting the scaffolding theory of aging and cognition. *Neuropsychology Review, 24*(3), 355–370. https://doi.org/10.1007/s11065-014-9270-9.

Rohde, G. K., Barnett, A. S., Basser, P. J., Marenco, S., & Pierpaoli, C. (2004). Comprehensive approach for correction of motion and distortion in diffusion-weighted MRI. *Magnetic Resonance in Medicine, 51*(1), 103–114. https://doi.org/10.1002/mrm.10677.

Rosen, W. G., Mohs, R. C., & Davis, K. L. (1984). A new rating scale for Alzheimer's disease. *American Journal of Psychiatry, 141*(11), 1356–1364. https://doi.org/10.1176/ajp.141.11.1356.

Shaw, L. M., Vanderstichele, H., Knapik-Czajka, M., Clark, C. M., Aisen, P. S., Petersen, R. C., … Trojanowski, J. Q. (2009). Cerebrospinal fluid biomarker signature in Alzheimer's disease neuroimaging initiative subjects. *Annals of Neurology, 65*(4), 403–413. https://doi.org/10.1002/ana.21610.

Smith, R. E., Tournier, J. D., Calamante, F., & Connelly, A. (2012). Anatomically-constrained tractography: Improved diffusion MRI streamlines tractography through effective use of anatomical information. *NeuroImage, 62*(3), 1924–1938. https://doi.org/10.1016/j.neuroimage.2012.06.005.

Stargardt, A., Swaab, D. F., & Bossers, K. (2015). The storm before the quiet: Neuronal hyperactivity and Aβ in the presymptomatic stages of Alzheimer's disease. *Neurobiology of Aging, 36*(1), 1–11. https://doi.org/10.1016/j.neurobiolaging.2014.08.014.

Stern, Y. (2012). Cognitive reserve in ageing and Alzheimer's disease. *The Lancet Neurology, 11*(11), 1006–1012. https://doi.org/10.1016/S1474-4422(12)70191-6.

Teipel, S. J., Meindl, T., Wagner, M., Kohl, T., Bürger, K., Reiser, M. F., Herpertz, S., Möller, H. J., & Hampel, H. (2009). White matter microstructure in relation to education in aging and Alzheimer's disease 1. *Journal of Alzheimer's Disease, 17*(3), 571–583. https://doi.org/10.3233/JAD-2009-1077.

Todorov, V., & Filzmoser, P. (2009). An object-oriented framework for robust multivariate analysis. *Journal of Statistical Software*. https://doi.org/10.18637/jss.v032.i03.

Tomasi, D., Wang, G.-J., & Volkow, N. D. (2013). Energetic cost of brain functional connectivity. *Proceedings of the National Academy of Sciences, 110*(33), 13642–13647. https://doi.org/10.1073/pnas.1303346110.

van den Heuvel, M. P., & Sporns, O. (2013). Network hubs in the human brain. *Trends in Cognitive Sciences, 17*(12), 683–696. https://doi.org/10.1016/j.tics.2013.09.012.

van den Heuvel, D. M. J., ten Dam, V. H., de Craen, A. J. M., Admiraal-Behloul, F., Olofsen, H., Bollen, E. L. E. M., et al. (2006). Increase in periventricular white matter hyperintensities parallels decline in mental processing speed in a non-demented elderly population. *Journal of Neurology, Neurosurgery & Psychiatry, 77*(2), 149–153. https://doi.org/10.1136/jnnp.2005.070193.

Watts, D. J., & Strogatz, S. H. (1998). Collective dynamics of 'small-world' networks. *Nature, 393*(6684), 440–442. https://doi.org/10.1038/30918.

Wolf, D., Fischer, F. U., & Fellgiebel, A. (2018). A methodological approach to studying resilience mechanisms: Demonstration of utility in age and Alzheimer's disease-related brain pathology. *Brain Imaging and Behavior*, 1–10. https://doi.org/10.1007/s11682-018-9870-8.

Wook Yoo, S., Han, C. E., Shin, J. S., Won Seo, S., Na, D. L., Kaiser, M., Jeong, Y., & Seong, J.-K. (2015). A network flow-based analysis of cognitive Reserve in Normal Ageing and Alzheimer's disease. *Scientific Reports, 5*, 10057. https://doi.org/10.1038/srep10057.

Zamora-López, G., Zhou, C., & Kurths, J. (2010). Cortical hubs form a module for multisensory integration on top of the hierarchy of cortical networks. *Frontiers in Neuroinformatics, 4*. https://doi.org/10.3389/neuro.11.001.2010.